Designing unit cell in three-dimensional periodic nanostructures using colloidal lithography

Joong-Hee Min, Xu A. Zhang and Chih-Hao Chang*

Department of Mechanical and Aerospace Engineering, North Carolina State University, Raleigh, North Carolina 27695, USA

*chichang@ncsu.edu

Abstract: Colloidal phase-shift lithography, the illumination of a two-dimensional (2D) ordered array of self-assembled colloidal nanospheres, is an effective method for the fabrication of periodic three-dimensional (3D) nanostructures. In this work, we investigate the design and control of the unit-cell geometry by examining the relative ratio of the illumination wavelength and colloidal nanosphere diameter. Using analytical and finite-difference time-domain (FDTD) modeling, we examine the effect of the wavelength-diameter ratio on intensity pattern, lattice constants, and unit-cell geometry. These models were validated by experimental fabrication for various combination of wavelength and colloid diameter. The developed models and fabrication tools can facilitate the design and engineering of 3D periodic nanostructure for photonic crystals, volumetric electrodes, and porous materials.

OCIS codes: (050.6875) Three-dimensional fabrication; (220.3740) Lithography; (220.4241) Nanostructure fabrication.

References and links

1. S. Y. Lin, J. G. Fleming, D. L. Hetherington, B. K. Smith, R. Biswas, K. M. Ho, M. M. Sigalas, W. Zubrzycki, S. R. Kurtz, and J. Bur, "A three-dimensional photonic crystal operating at infrared wavelengths," Nature **394**, 251–253 (1998).
2. S. Noda, K. Tomoda, N. Yamamoto, and A. Chutinan, "Full Three-dimensional photonic bandgap crystals at near-infrared wavelengths," Science **289**(5479), 604–606 (2000).
3. D. Mei, B. Cheng, W. Hu, Z. Li, and D. Zhang, "Three-dimensional ordered patterns by light interference," Opt. Lett. **20**(5), 429–431 (1995).
4. T. Gorishnyy, C. K. Ullal, M. Maldovan, G. Fytas, and E. L. Thomas, "Hypersonic phononic crystals," Phys. Rev. Lett. **94**(11), 115501 (2005).
5. J.-H. Jang, C. K. Ullal, T. Choi, M. C. Lemieux, V. V. Tsukruk, and E. L. Thomas, "3D polymer microframes that exploit length-scale-dependent mechanical behavior," Adv. Mater. **18**(16), 2123–2127 (2006).
6. J.-W. Jang, Z. Zheng, O.-S. Lee, W. Shim, G. Zheng, G. C. Schatz, and C. A. Mirkin, "Arrays of nanoscale lenses for subwavelength optical lithography," Nano Lett. **10**(11), 4399–4404 (2010).
7. I. Wathuthanthri, Y. Liu, K. Du, W. Xu, and C.-H. Choi, "Simple holographic patterning for high-aspect-ratio three-dimensional nanostructures with large coverage area," Adv. Funct. Mater. **23**(5), 608–618 (2013).
8. X. A. Zhang, A. Bagal, E. C. Dandley, J. Zhao, C. J. Oldham, B. Wu, G. N. Parsons, and C. Chang, "Ordered 3D thin-shell nanolattice materials with near-unity refractive Indices," Adv. Funct. Mater. **25**(42) 6644–6649 (2015).
9. S. Jeon, J.-U. Park, R. Cirelli, S. Yang, C. E. Heitzman, P. V. Braun, P. J. Kenis, and J. A. Rogers, "Fabricating complex three-dimensional nanostructures with high-resolution conformable phase masks," Proc. Natl. Acad. Sci. U.S.A. **101**(34), 12428–12433 (2004).
10. J.-H. Jang, C. K. Ullal, M. Maldovan, T. Gorishnyy, S. Kooi, C. Koh, and E. L. Thomas, "3D micro- and nanostructures via interference lithography," Adv. Funct. Mater. **17**(16), 3027–3041 (2007).
11. D. J. Shir, S. Jeon, H. Liao, M. Highland, D. G. Cahill, M. F. Su, I. F. El-Kady, C. G. Christodoulou, G. R. Bogart, A. V. Hamza, and J. A. Rogers, "Three-dimensional nanofabrication with elastomeric phase masks," J. Phys. Chem. B **111**(45), 12945–12958 (2007).
12. J. Park, S. Yoon, K. Kang, and S. Jeon, "Antireflection behavior of multidimensional nanostructures patterned using a conformable elastomeric phase mask in a single exposure step," Small **6**(18), 1981–1985 (2010).
13. Y. S. Nam, S. Jeon, D. J. Shir, A. Hamza, and J. A. Rogers, "Thick, three-dimensional nanoporous density-graded materials formed by optical exposures of photopolymers with controlled levels of absorption," Appl. Opt. **46**(25), 6350–6354 (2007).

#247983 Received 21 Aug 2015; revised 28 Oct 2015; accepted 18 Nov 2015; published 21 Dec 2015

14. M. K. Kwak, J. G. Ok, J. Y. Lee, and L. J. Guo, "Continuous phase-shift lithography with a roll-type mask and application to transparent conductor fabrication," Nanotechnology **23**(34), 344008 (2012).
15. J. K. Hyun, J. Park, E. Kim, L. J. Lauhon, and S. Jeon, "Rational control of diffraction and interference from conformal phase gratings: toward high-resolution 3D nanopatterning," Adv. Opt. Mater. **2**(12), 1213–1220 (2014).
16. H. H. Solak, C. Dais, and F. Clube, "Displacement Talbot lithography: a new method for high-resolution patterning of large areas," Opt. Express **19**(11), 10686–10691 (2011).
17. C. H. Chang, L. Tian, W. R. Hesse, H. Gao, H. J. Choi, J. G. Kim, M. Siddiqui, and G. Barbastathis, "From two-dimensional colloidal self-assembly to three-dimensional nanolithography," Nano Lett. **11**(6), 2533–2537 (2011).
18. J. C. Hulteen, "Nanosphere lithography: A materials general fabrication process for periodic particle array surfaces," J. Vac. Sci. Technol. A Vacuum, Surfaces, Film. **13**, 1553 (1995).
19. X. A. Zhang, J. Elek, and C.-H. Chang, "Three-dimensional nanolithography using light scattering from colloidal particles," ACS Nano **7**(7), 6212–6218 (2013).
20. X. A. Zhang, B. Dai, Z. Xu, and C.-H. Chang, "Sculpting asymmetric, hollow-core, three-dimensional nanostructures using colloidal particles," Small **11**(11), 1285–1292 (2015).
21. J. E. Elek, X. A. Zhang, B. Dai, Z. Xu, and C.-H. Chang, "Fabrication of three-dimensional hierarchical nanostructures using template-directed colloidal assembly," Nanoscale **7**(10), 4406–4410 (2015).
22. S.-G. Park, T. Y. Jeon, H. C. Jeon, S.-M. Yang, J.-D. Kwon, C.-W. Mun, B. Cho, C. S. Kim, and D.-H. Kim, "Fabrication of 3D ZnO hollow shell structures by prism holographic lithography and atomic layer deposition," J. Mater. Chem. C Mater. Opt. Electron. Devices **2**(11), 1957 (2014).
23. T. Y. Jeon, H. C. Jeon, S. Y. Lee, T. S. Shim, J.-D. Kwon, S.-G. Park, and S.-M. Yang, "3D hierarchical architectures prepared by single exposure through a highly durable colloidal phase mask," Adv. Mater. **26**(9), 1422–1426 (2014).
24. M. Fang, H. Lin, H.-Y. Cheung, F. Xiu, L. Shen, S. Yip, E. Y.-B. Pun, C.-Y. Wong, and J. C. Ho, "Polymer-confined colloidal monolayer: a reusable soft photomask for rapid wafer-scale nanopatterning," ACS Appl. Mater. Interfaces **6**(23), 20837–20841 (2014).
25. C. Geng, Q. Yan, C. Du, P. Dong, L. Zhang, T. Wei, Z. Hao, X. Wang, and D. Shen, "Large-Area and Ordered Sexfoil Pore Arrays by Spherical-Lens Photolithography," ACS Photonics **1**(8), 754–760 (2014).
26. H. F. Talbot, "LXXVI. Facts relating to optical science. No. IV," Philos. Mag. Ser. 3 **9**, 401–407 (1836).
27. L. Rayleigh, "XXV. On copying diffraction-gratings, and on some phenomena connected therewith," Philos, Mag. Ser. 5 **11**(67), 196–205 (1881).
28. J. Wen, Y. Zhang, and M. Xiao, "The Talbot effect: recent advances in classical optics, nonlinear optics, and quantum optics," Adv. Opt. Photonics **5**(1), 83 (2013).
29. J. T. Winthrop and C. R. Worthington, "Theory of fresnel images. i. plane periodic objects in monochromatic light," J. Opt. Soc. Am. **55**(4), 373–381 (1965).
30. A. Isoyan, F. Jiang, Y. C. Cheng, F. Cerrina, P. Wachulak, L. Urbanski, J. Rocca, C. Menoni, and M. Marconi, "Talbot lithography: Self-imaging of complex structures," J. Vac. Sci. Technol. B Microelectron, Nanom. Struct. **27**, 2931 (2009).
31. M.-S. Kim, T. Scharf, C. Menzel, C. Rockstuhl, and H. P. Herzig, "Talbot images of wavelength-scale amplitude gratings," Opt. Express **20**(5), 4903–4920 (2012).
32. A. F. Oskooi, D. Roundy, M. Ibanescu, P. Bermel, J. D. Joannopoulos, and S. G. Johnson, "Meep: A flexible free-software package for electromagnetic simulations by the FDTD method," Comput. Phys. Commun. **181**(3), 687–702 (2010).
33. J. Li, Y. Cho, I.-S. Choi, and S. Yang, "Transforming one-dimensional nanowalls to long-range ordered two-dimensional nanowaves: exploiting buckling instability and nanofibers effect in holographic lithography," Adv. Funct. Mater. **24**(16), 2361–2366 (2014).

1. Introduction

Periodic three-dimensional (3D) nanostructures have many interesting applications in photonic materials, microbatteries, fluidic filters, and metamaterials [1–9]. One effective method to fabricate 3D nanostructure is phase-shift lithography, where an optical phase element diffracts normal incident light and generates a 3D intensity distribution in close proximity. The optical pattern is governed by the Talbot effect, and can be recorded by photoresist [9–16]. Such method has been employed by various groups, where a conformal polydimethylsiloxane (PDMS) mask is used to pattern periodic 3D nanostructures. However, in these processes it is important that a high-quality mold is used for the PDMS mask, which typically requires use of expensive and time-consuming fabrication processes such as deep-ultraviolet, electron-beam, and atomic force lithography followed by plasma dry etching.

Another method to implement phase-shift lithography is using a 2D colloidal nanosphere array, which replaces the PDMS mask as the optical diffractive element [17]. In this scheme,

#247983 Received 21 Aug 2015; revised 28 Oct 2015; accepted 18 Nov 2015; published 21 Dec 2015

the colloidal sphere arrays act as a periodic phase element to generate periodic Talbot patterns, eliminating the need for physical masks. The nanospheres can be also be assembled into a regular pattern [18] directly on the photoresist, reducing fabrication complexity and other close-contact issue involved in masks. It is also possible to control the lattice parameters in all three directions by controlling sphere diameter and illuminating wavelength. This approach provides a low-cost method for the scalable fabrication of 3D periodic nanostructures. The use of colloids can also enable other complex geometry, including nano-volcano arrays [19,20], 3D hierarchical nanostructures [21], and other colloidal-assisted lithography [22–25].

In this work, we investigate the design of feature geometries within a 3D nanostructure unit cell in colloidal phase lithography. This is accomplished by examining the illumination wavelength normalized by the wavelength, which leads to a unitless parameter. Using analytical modeling, the Talbot distance and sub-image planes of the periodic intensity patterns can be examined. This is then compared to a numerical model using finite-different time-domain (FDTD) methods, which will provide a design map on the influence of the wavelength-diameter ratio on the unit-cell geometry. The analytical and numerical models are confirmed by experimental fabrication, and the error will be studied.

2. Colloidal lithography and Talbot effect

Colloidal phase lithography is based on the well-known Talbot effect, which occurs in the near field when a periodic pattern is illuminated with normal incidence light [26–28]. A schematic of this system is illustrated in Fig. 1, where a cross-section particle array and its simulated intensity using FDTD are overlaid. Orthogonal cross sections in both x and y directions are examined to investigate the 3D intensity distribution. The wavelength and sphere diameters are 105 nm and 500 nm, respectively. The Talbot distance (z_t), or one period of the periodic Talbot pattern in the axial direction as noted, can be calculated by the equation below,

$$z_t = \frac{\frac{\lambda}{n}}{1-\sqrt{1-\left(\frac{\lambda}{n\Lambda}\right)^2}}. \tag{1}$$

where λ is the wavelength of incident light, n is the refractive index of propagating medium, and D is the diameter of colloidal particle in this equation. Note that the lateral period, $\Lambda = D\sqrt{3}/2$ because the colloidal spheres form a hexagonal array [29–31]. The Talbot distance can be normalized by the lateral period, and defining the unitless parameter $\gamma = \lambda / n\Lambda$ yields,

$$\frac{z_t}{\Lambda} = \frac{\gamma}{1-\sqrt{1-\gamma^2}}. \tag{2}$$

Note the normalized Talbot distance is governed only by γ, therefore it is the sole factor in defining and controlling the longitudinal lattice constant of the generated 3D periodic nanostructure [17]. Beyond the lattice constant, the γ parameter also determines the diffraction order allowed to propagate in the photoresist. Higher $\gamma > 1/\sqrt{3}$ allows only 0th and 1st diffraction orders (m = 1), resulting in simpler periodic patterns, while lower $\gamma > 1/\sqrt{7}$ makes more complex Talbot patterns with higher diffraction orders (m > 2), yielding multiple sub-image planes [17]. The existence of the sub-images results in higher spatial frequency features within a unit cell then specified by the lattice parameter. Therefore, a variety 3D periodic nanostructure with different geometry can be generated simply by varying γ

#247983 Received 21 Aug 2015; revised 28 Oct 2015; accepted 18 Nov 2015; published 21 Dec 2015

parameter through different combinations of wavelengths and colloidal particle diameters. This approach enabled the design and control of feature geometry within a single unit cell.

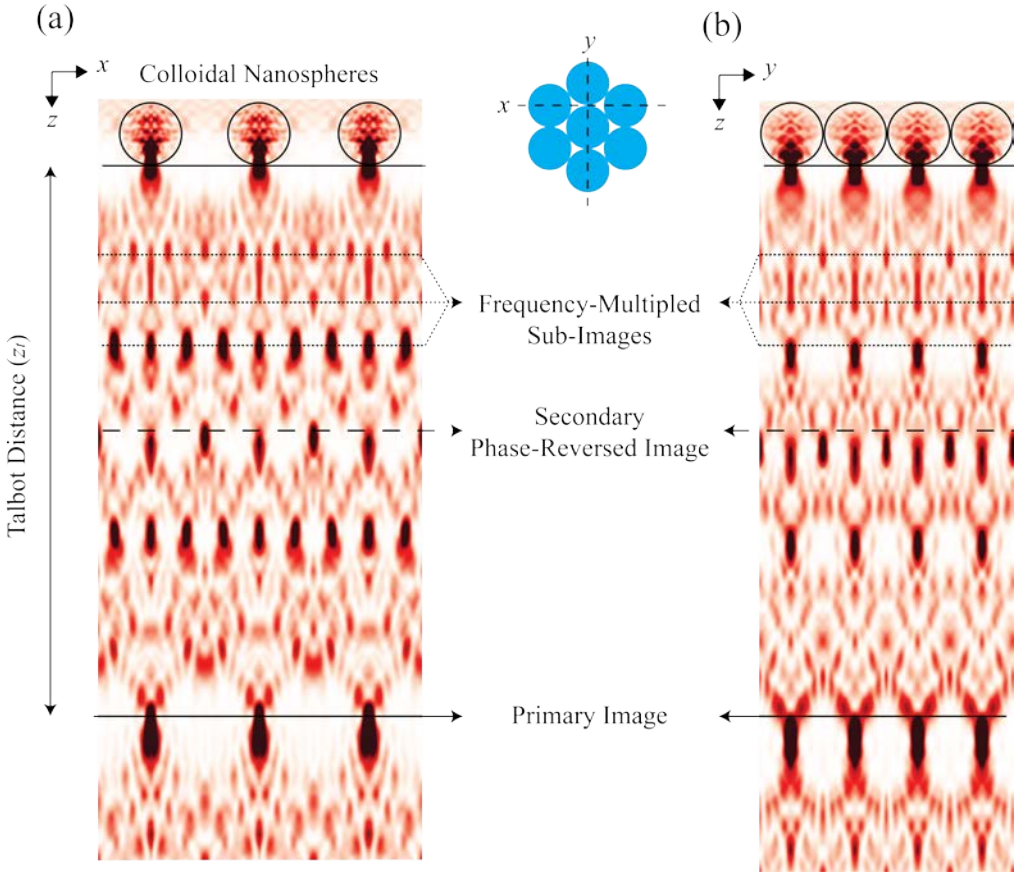

Fig. 1. The simulated intensity cross-sections by FDTD along with (a) x-direction and (b) y-direction of colloidal nanosphere hexagonal array

Using FDTD method [32], the periodic optical intensity profile can be studied to optimize the 3D exposure parameters. Simulation results of γ = 0.1 to 0.9 with a step of 0.05 are shown in Fig. 2. The index and diameter of the sphere were kept constant at n = 1.67 and 500 nm, respectively, and the gamma values were obtained by varying wavelengths. It can be observed that higher γ results in simpler intensity patterns, while lower $\gamma < 1/\sqrt{7}$ shows well-defined Talbot sub-images, such as a primary image at z_t, a phase-reversed image at roughly $z_t/2$, and multiple frequency-multiplied images within one Talbot period. Below $\gamma = 1/\sqrt{3}$, various sub-images were observed and defined readily due to multiple diffraction orders (m > 1). However when $\gamma > 1/\sqrt{3}$, only primary and secondary phase-reversed images can be observed and they repeat in the axial direction, as predicted by the Talbot effect.

To analyze the features in more details, the corresponding unit cells from each intensity pattern were extracted, normalized in the axial direction, and compared in lower side of Fig. 2. For γ < 0.2, the unit cells contain complex features with higher spatial frequencies due to multiple sub-image planes. The Talbot distance also increases significantly to several multiples of the longitudinal lattice spacing, making the unit cell highly elongated in the axial direction. On the other hand, the intensity profiles in higher range of γ > 0.6 showed simpler periodic patterns. Simple unit-cell geometries in this regime will lead to facile control over

#247983 Received 21 Aug 2015; revised 28 Oct 2015; accepted 18 Nov 2015; published 21 Dec 2015

height and width of constituent elements by choosing proper sphere size and wavelength. In this regime the structures have uniform pore sizes and can find applications in photonics and nanostructured materials. In the intermediate range where $0.2 < \gamma < 0.6$, the unit cells have complex intensity profile but presented fewer sub-images that are dominant. In this case fabrication of the structure is more feasible.

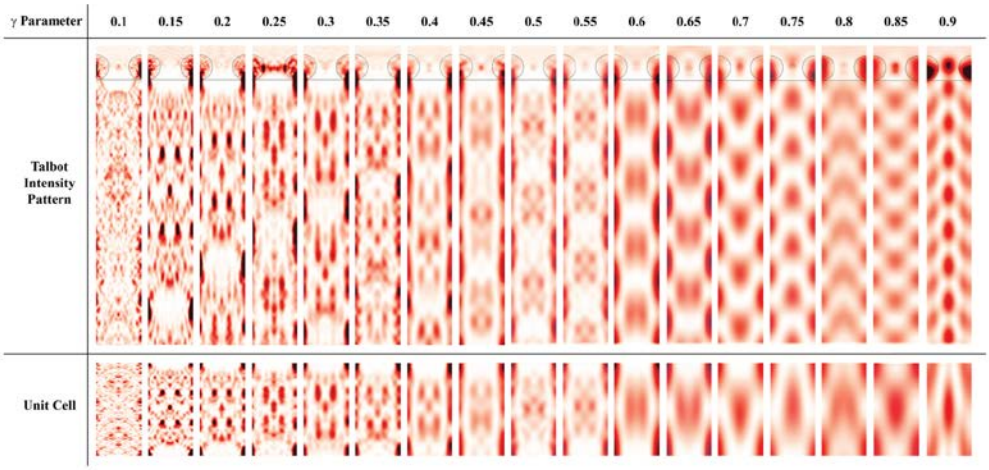

Fig. 2. Numerical FDTD simulation of Talbot intensity pattern for colloidal phase shift lithography under normal illumination. The γ parameter is varied from 0.1 to 0.9, resulting in different unit-cell geometries. Lower γ parameter results show various Talbot sub-images including frequency-doubled and -tripled fractional images. Only primary and secondary images can be observed at higher γ parameter.

3. Fabrication process

The fabrication process for colloidal phase-shift lithography using assembled nanospheres is illustrated in Fig. 3. For all experiments, anti-reflection coating (ARC i-CON-7, Brewer Science, Inc.) was spin-coated on a silicon wafer to prevent reflection during lithography. SU-8 (Microchem, Corp.), a negative photoresist was selected for its relatively low optical absorption to enable thick structures. To promote adhesion between ARC and SU-8, an SU-8 buffer layer of 500 nm was used. The buffer layer was flood-exposure (200 mJ/cm^2) and hard-baked at 220 °C for 5 minutes. Then, a target layer of SU-8 with controlled thickness (5~7 μm) was spin-coated on top of the buffer layer and soft-baked at 95 °C. A monolayer of 2D polystyrene nanosphere array with various ranges of sphere diameter (D = 350~1000 nm, Polyscience Polybead Microspheres in 2.5% aqueous solution) was assembled on top of the photoresist layer, as shown is a cross-sectional SEM image in Fig. 3(a). The exposure process was performed with 3 different light sources, a HeCd laser (λ = 325 nm), a mercury lamp with bandpass filter (centered at λ = 365 nm), and a laser diode module (λ = 405 nm). The exposure dose differs for the light sources due to the difference in light absorption coefficient of SU-8 at different wavelength. The dose was about 4~8 mJ/cm^2 for λ = 325 nm, and 50~100 mJ/cm^2 for λ = 365 and 405 nm. A photo-initiator cyclopentadienyl(fluorene) iron(II) hexafluoro-phosphate (Sigma-Aldrich) was added to SU-8 for λ = 405 nm exposure to increase resist sensitivity.

After exposure, the colloidal spheres were removed using ultrasonication system, and the post-exposure bake step was conducted at around 70 °C for 5 minutes. The resulting structure is shown in Fig. 3(b), and some material shrinkage due to polymer crosslinking can be observed. The sample was then developed with propylene glycol monomethyl ether acetate (PGMEA) and the rinsed in isopropyl alcohol (IPA). The final 3D periodic nanostructure is shown in Fig. 3(c), which has multiple periods of Talbot patterns within about 5~6 μm of

#247983 Received 21 Aug 2015; revised 28 Oct 2015; accepted 18 Nov 2015; published 21 Dec 2015

thickness. The fabrication parameters, especially exposure dose, post-exposure bake temperature and time were optimized experimentally to confirm well-organized and durable 3D periodic nanostructures.

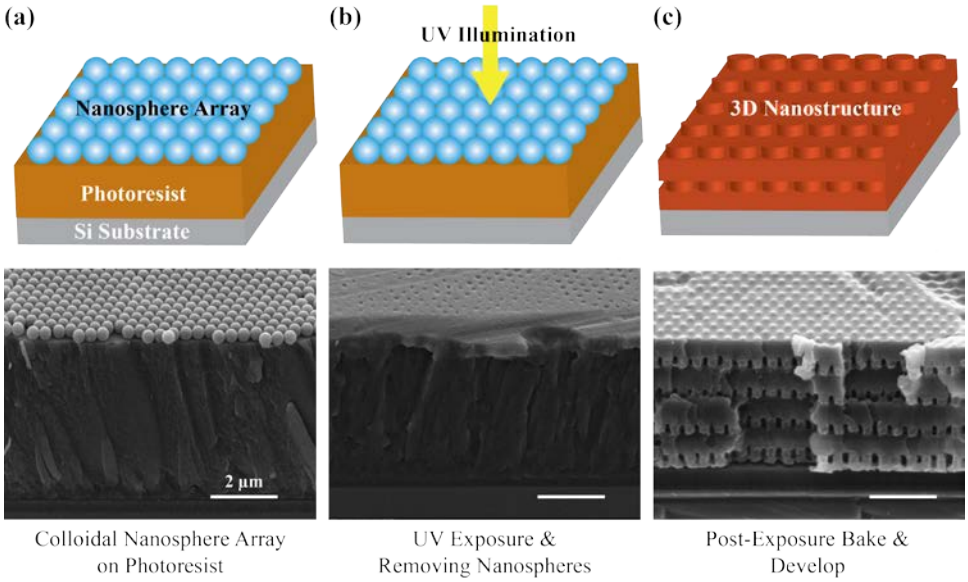

Fig. 3. Fabrication Process and SEM Images with scale bars of 2 μm. (a) Preparation of 2D self-assembled colloidal nanosphere array on photoresist layer; (b) UV exposure over 2D colloidal mask and removal of nanospheres; (c) Development of photoresist and final 3D periodic nanostructure

4. Experimental results

Based on the analytical and numerical models, different combinations of incident light wavelengths and sphere sizes can be utilized to control the γ parameter and demonstrate various types of 3D nanostructures. According to Eq. (2), longer wavelength and smaller diameter of sphere results in higher γ parameter, and vice versa. 3D nanostructures with γ = 0.23 to 0.65 were experimentally fabricated, as shown in Fig. 4. The FDTD simulation data for the corresponding γ parameter are also shown, and agrees well with experimental results. From the analysis in the previous section, the most complex 3D patterns were achieved at low $\gamma < 1/\sqrt{7}$, which results higher diffraction order was allowed in this case. Note that a thin layer on top of every structures was generated while the oxygen plasma surface treatment step for assembling colloidal nanospheres on SU-8. In the fabricated structure with γ = 0.31, the frequency-doubled sub-image plane can be observed at 992 nm and the feature period is around 360 nm, which is less than half of the sphere period. The γ = 0.23 case was expected to generate more complex fabricated 3D structures, however the finer features by the frequency-multipled sub-images did not develop. This can be attributed to lower exposure contrast in those areas, and resulted in fully crosslinked layer. The first frequency-multiplied sub-image plane, on the other hand, can still be observed and has feature period of about 500 nm. When γ parameter is higher than $1/\sqrt{7}$, the fabricated nanostructures showed simpler unit cell and more robust structures because the primary images were repeated with much shorter period while the sub-images do not exist. The most durable structures were achieved at γ = 0.58, where the thickness of its column and plane were almost the same everywhere inside the structure.

Some structural collapse and breakage can be observed for structures fabricated using a mercury lamp with a 365 nm bandpass filter. We believe this is due to the finite bandpass

#247983 Received 21 Aug 2015; revised 28 Oct 2015; accepted 18 Nov 2015; published 21 Dec 2015

bandwidth, which is about 10 nm. As a result the Talbot image is blurred, reducing exposure contrast and leading to collapse during development. This shows that while not required, single-wavelength laser sources are preferred when fabricating robust 3D nanostructures. In addition, the exposure using 405 nm laser diode module (γ = 0.57) showed many partial collapses or breaks than other fabrication results. This can be due to the chemistry incompatibility of the photo-initiator to enhance sensitivity. The process optimization of the ratio of photo-initiator to SU-8 solution is currently underway to avoid these defects due to the incomplete cross-linking.

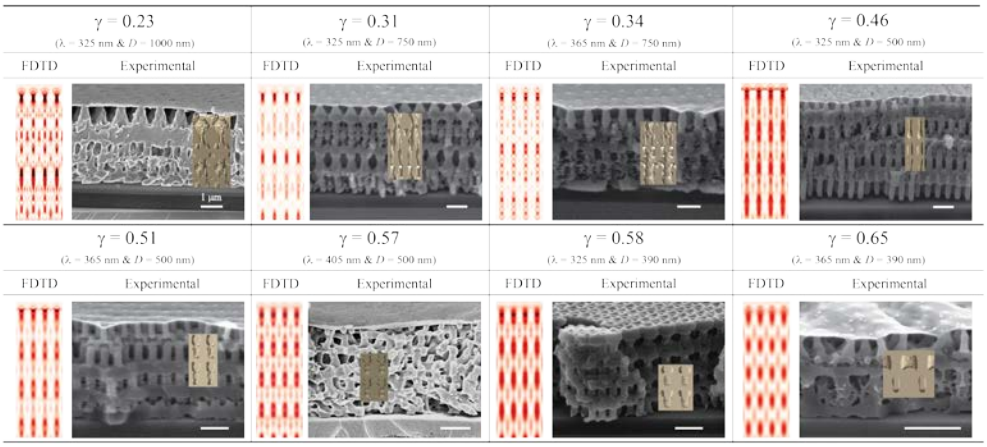

Fig. 4. Comparison of FDTD simulations and experimental results with various γ parameters. Lower γ (0.23 and 0.31) shows complex patterns, and higher γ (0.58 and 0.65) results in simple patterns. Scale bars in every SEM images indicate 1 μm.

Another limitation of our work came from the nature of SU-8, which requires a post-exposure bake step to crosslink the polymer and swells during development [33]. Although the baking process was optimized experimentally to obtain structures with high quality, the swelling issue cannot be resolved thoroughly and resulted in mechanical instability of 3D nanostructure. This occasionally leads structural failure during aqueous rinsing and drying step due to the surface tension. However this limitation can be mitigated by using critical point drying. Structures with finer features and physical defects are much vulnerable to this issue, and we believe this explains why the lower γ nanostructure was more difficult to obtain experimentally because they typically contain multiple frequency-multiplied sub-images.

Lastly, the dependency of the normalized Talbot distance, z_t/Λ on γ parameter for the fabricated nanostructures are compared with analytical and FDTD models, as depicted in Fig. 5. The different diffraction regimes are also identified, where m = 1, m = 2, and m > 2 results in Talbot patterns with secondary phase-reversed image, single sub-image plane, and multiple sub-image planes, respectively. In general, both the analytical and FDTD models agree well with the experimental data and less than 5% of error was observed in most range of γ. However for γ < 0.3, the analytical and FDTD models diverge slightly, and the experimental data shows better agreement to the analytical model. One possible reason is that the FDTD model resulted in high-frequency intensity fluctuation due to near-field effect at nanosphere array and photoresist interface, which made it difficult to determine the exact Talbot distance from the following repeated patterns. Also, the higher errors among experimental data were mainly from the samples with a bandpass filter, which is explainable by the dispersed wavelength after the bandpass filter, leading to structure collapse. The sample with the most partial collapse in the structure (γ = 0.57) also has the highest error, where the experimentally measured Talbot distance is 10.2% and 7.1% smaller than the analytical and numerical models, respectively. This is expected as the structure collapse reduced the overall structure

#247983 Received 21 Aug 2015; revised 28 Oct 2015; accepted 18 Nov 2015; published 21 Dec 2015

height. Other than that, the experimental data showed good agreement, and this demonstrates the unit cell in our 3D nanostructure is designable and controllable by selecting a proper γ parameter. The detailed comparison between analytical, numerical, and experimental data is shown in Table 1.

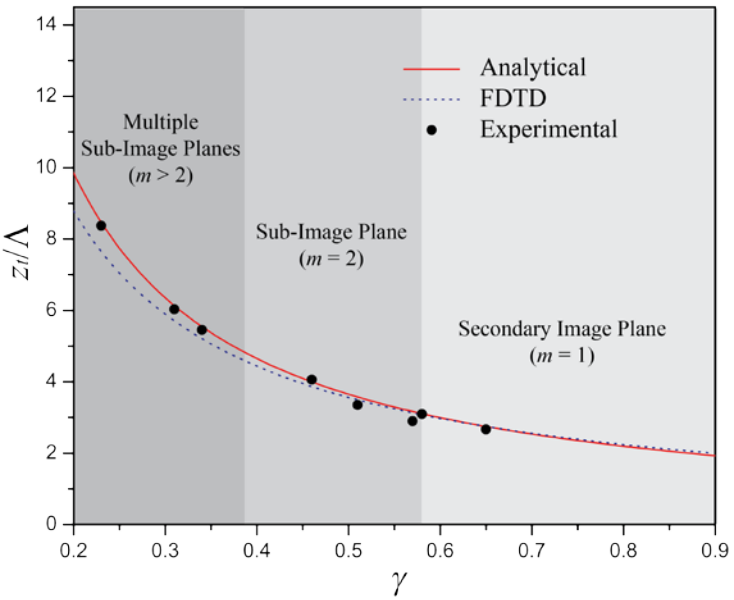

Fig. 5. Comparison of analytical, numerical (FDTD), and experimental values of normalized Talbot distance between γ = 0.2 and 0.9. The colored area shows the regions which m diffraction orders are allowed. The boundary values are $\gamma = 1/\sqrt{3}$ and $\gamma = 1/\sqrt{7}$.

Table 1. Analytical, numerical and experimental Talbot distance data with corresponding γ parameter.

γ Parameter	Experimental (nm)	Analytical (nm)	Error (%)	Numerical (nm)	Error (%)
0.65	901	908	0.8	908	0.8
0.58	1048	1053	0.5	1053	0.5
0.57	1254	1397	10.2	1350	7.1
0.51	1454	1581	8.0	1545	5.9
0.46	1764	1804	2.2	1683	–4.8
0.34	3547 (Primary)	3709	4.4	3350	–5.9
	885 (Doubled)			834	–6.1
0.31	3926 (Primary)	4193	6.4	3656	–7.4
	992 (Doubled)			914	–8.6
0.23	3630 (Secondary)	3767	3.6	3358	–8.1
	1850 (Doubled)			1679	–10.1

#247983 Received 21 Aug 2015; revised 28 Oct 2015; accepted 18 Nov 2015; published 21 Dec 2015

5. Conclusion

In this work we have demonstrated a method exploiting the Talbot effect generated by colloidal phase mask to design unit cell geometries for periodic 3D nanostructures. First, we analytically calculated Talbot distance and numerically simulated Talbot intensity patterns for a wide range of unitless parameter, γ. Then, using a 2D self-assembled polystyrene nanosphere array as a phase shift mask, 3D nanostructures were successfully fabricated within a thick negative-tone photoresist. The γ parameter was the sole factor to control the lattice parameters, unit-cell feature sizes, and complexity of intermediate sub layers, and different nanostructures were achieved experimentally by various combinations of incident light wavelengths and nanosphere sizes. The experimental results were compared with analytical and numerical models, and it showed a good agreement with less than 5% error in most of cases. Both complex unit cell with lower γ and simple unit cell with higher γ are expected to be useful in practical applications, such as photonic crystals, microfluidics, and ordered cellular materials.

Acknowledgments

We gratefully acknowledge the students, staff, and facility support from the North Carolina State University Nanofabrication Facility (NNF). The authors also acknowledge the use of the Analytical Instrumentation Facility (AIF) at North Carolina State University, which is supported by the State of North Carolina and the National Science Foundation (NSF). This work was supported by a NASA Office of the Chief Technologist's Space Technology Research Opportunity – Early Career Faculty grant (grant NNX12AQ46G).

#247983 Received 21 Aug 2015; revised 28 Oct 2015; accepted 18 Nov 2015; published 21 Dec 2015